J Ther Eng, Vol. 12, No. 2, pp. 815−829, March, 2026

Journal of Thermal Engineering
Web page info: https://jten.yildiz.edu.tr
DOI: 10.14744/thermal.0001113

Review Article

Simulation of the thermal marangoni effect in a free surface cavity: Heatline and entropy visualizations

Nagham Yass KHUDAIR[1], Qusay Rasheed AL-AMIR[2], Hayder K. RASHID[3]

[1]Department Metallurgy Engineering, College of Material Engineering, University of Babylon, Hilla, Iraq
[2]Department of Mechanical Power Technical Engineering, College of Engineering and Technology, Al-Mustaqbal University, Hilla, Babylon, Iraq
[3]Department of Ceramic Engineering, College of Material Engineering, University of Babylon, Hilla, Iraq

ARTICLE INFO

Article history
Received: 16 January 2025
Revised: 25 April 2025
Accepted: 01 August 2025

Keywords:
Marangoni Convection; Cavity; FVM; Heat Function; Entropy Generation

ABSTRACT

There are many modern engineering applications of natural convection with free surface square cavity. In this paper analyzes numerically convection that is both natural and Marangoni. Together adiabatic cooling and convective cooling are subject to the upper free surface boundary, whereas a portion of the bottom wall boundary is exposed to constant heat flux and the remaining portions are maintained adiabatically. The unique of this research is the possibility of using its numerical analysis to enhance the applications related to solar energy, which is considered one of the most important applications in the field of renewable energy, in addition to food storage**.** The boundaries of the vertical walls of square cavity are kept cold. Under the influence of constant heat flux, two physical phenomena thermocapillary and buoyancy forces are considered and statistically depicted. A finite volume method is used to solve the governing equations based on the heat line approach. The current research is supported by other studies that are published in the literature. For different values of the Marangoni number (-10^3 to $+10^4$), Grashof number (10^4 to 10^5), Prandtl number (0.054, 0.16, 0.71, 6.2, 100), and Biot number (0 to 80) are produced to investigate the impacts on streamlines, isothermal lines, heat lines, and local entropy generation. The solving of the government equations is depending on numerical solution for the control volume system with assumed that the situation of heat transfer and fluid flow is steady with generating entropy over the all-control volume under investigation and density differences are ignored. It has been noted that the maximum stream function increases as Marangoni numbers increase from 0 to 10^4. This trend results from the fact that the flow velocity increases with the increasing Marangoni number. However, the Marangoni It has a reciprocal effect with convective heat transfer. The solution and its improvement are within the conditions of this research. The flow pattern is not considerably affected when the Biot number is changed from 40 to 80 as the surface tension is minimal.

Cite this article as: Khudair NY, Al-Amir QR, Rashid HK. Simulation of the thermal marangoni effect in a free surface cavity: heatline and entropy visualizations. J Ther Eng 2026;12(2):815−829.

***Corresponding author.**
*E-mail address: mat.hayder.k@uobabylon.edu.iq

This paper was recommended for publication in revised form by Editorin-Chief Ahmet Selim Dalkılıç

INTRODUCTION

The influence of buoyancy and thermocapillary forces on heat transfer in free surface cavities were received extensive study in recent years. The range of industrial processes, including drying and crystal development melting, was what sparked this curiosity. Surface tension differences at a liquid-gas interface brought on by temperature differences generate fluid motion at the free surface. Marangoni convection or Thermocapillary flow is the technical term for such motion. Besides, fluid motion can also be brought on by the buoyancy force. The convective flow was steered in the opposite direction by the combined forces of thermocapillary and buoyancy [1]. A little amount of a surface-active contaminant was found to be the cause of the thermocapillary flow's anomalous direction [2].

Reviewing relevant earlier work reveals that the majority of them [3–15] focused on thermocapillary convection and combined buoyancy in cavities with differential heating. According to Saleh et al. [3] investigated cooling intensity for any fluid type results in an increase in the amount of heat transfer at the hot wall and a decrease at the cold wall. In a computational analysis of constant convective flow in a square cavity, Bergman and Ramadhyani [4] demonstrated how surface tension effects can drastically change the buoyancy-induced flow. For different Rayleigh numbers, Cicek and Baytas [5] have been looked at the impact of a negative and positive Marangoni number on heat transfer and fluid flow. Strani et al. [6] have been concluded that for low crispation numbers, the surface deformation had no impact on the qualitative characteristics of the flow field structure. The heat lines approach was used by Arbin et al. [7] to investigate the double-diffusive natural convection inside an open-topped square cavity that was differentially heated. They demonstrated how the heater segment length affects the mechanisms of heat and mass transfer. Buoyancy ratio, surface tension, and the heater segment all play a role in the heat transfer, fluid flow, and concentration distribution within the cavity. Jue [8] demonstrated how concentration and temperature contribute to the flow in opposite ways and how their distributions along the surface boundary exhibit local variation. In the presence of a magnetic field, Rudraiah et al. [9] investigated buoyancy and thermocapillary induced flow. They said that while heat transfer diminishes in the presence of a magnetic field, it increases with the Marangoni number. Also, research by Saleem et al. [10] conducted investigations to study the double-diffusive convection in presence of a magnetic field inside a square cavity. The results demonstrated that while the heat and mass transfer rates increase with an increase in the parameter of chemical reaction, the average Sherwood number and the average Nusselt number drop with increasing values of Hartmann number. Furthermore, concentration buoyancy has a higher influence on flow than thermal buoyancy does.

Additionally, Hossain et al. [11] investigated how an external magnetic field affected combined buoyancy and thermocapillary convection flow while also taking into account the impact of internal heat generation. The study of natural convection is significant due to the irreversibility phenomena caused by fluid friction and heat transfer that are reflected by entropy generation. In a cubical cavity, the coupled three-dimensional buoyancy and thermocapillary convection were solved by Oztop et al. [12]. For lower values of Rayleigh numbers, they discovered that the number of Marangoni becomes a more powerful parameter on total entropy generation.

Saleh and Hashim [13] investigated how different nanoparticle kinds and concentrations affected buoyant Marangoni convection in a square cavity that was variably heated. They concluded that when convective thermocapillary and buoyancy forces are equivalent in strength, a rise in nanoparticle concentration results in a drop in flow rates in secondary cells. The magnitudes of the Grashof number and Prandtl number to be related to the active spot of greatest entropy formation have been shown by Saleem et al. [14]. The rate of entropy creation rises as the Marangoni number rises. The visualization of heat flow and the formation of entropy during natural convection in inclined square cavities were studied by Basak et al. [15] more recently using a finite element simulation. Their result illustrated that high rates of heat transfer with low entropy generation occur regardless of the Prandtl number. In a rectangular cavity with vertical walls that were heated differently, Ilis et al. [16] studied the impact of aspect ratio on the formation of entropy owing to natural convection. The entropy generation during natural convection in a rectangular inclined enclosure was explored numerically by Bouabid et al. [17]. They concluded that the thermal Grashof number, cavity aspect ratio, and irreversibility distribution ratio all rise with increasing amounts of entropy. In lid-driven enclosures filled with a porous media, several convection modes, entropy generation caused by Marangoni effects, side wall movement, and double-diffusive convection are studied by Ahmed et al. [18]. The average Bejan number is found to drop by 4.77% as the Bingham number increases from 0 to 0.5. Kolsi et al. [19] studied the effects of inserting a Carbon Nano Tube and providing a magnetic field on the 3D-thermocapillary natural convection. The findings showed that raising the volume fraction of nanoparticles and changing the magnetic field's strength and direction have a significant impact on the rate of heat transfer and flow structure. In a different study, Basak et al. [20] investigated the formation of entropy by natural convection in right-angled triangle cavities having porous media and top angles between 15° and 45° under varied temperature boundary conditions. A new method was used by Joe Bobach et al. [21] to simulate and validate the surface tension and phase change phenomena within a square space. This method is based on the particle finite element theory and was employed to simulate a series of test cases. Moreover, Zailan et al. [22] conducted numerical study for carried out the effect of Marangoni convection (Ma) with

in two-dimensional C type enclosure contained the nanofluid. Where, the COMSOL program software are used for numerical solutions. The observed that, the strength of the flow increases with Ma. Moreover, Zisan et al. [23] numerically investigated the Marangoni natural convection with in a three-dimensional enclosure located a pair of discrete heaters at the bottom and insulated the rest with insulation the top too. Using the finite element method for solving the Navier-Stokes and energy equations. They observed that the shear stress builds up due to the surface tension gradient and causes to initiate an additional vortex. On the other hand, Muhammad et al. [24] conducted a numerical investigation of a trapezoidal enclosure with a circular heated cylinder with fluid-flow and heat transfer rate of nanofluid inside. They found that the Rayleigh and Marangoni number were signification the strength of the flow. Also, Omer [25] studied the Marangoni convection problem for hybrid nanofluids. They using numerically to solve the partial differential equation by Matlab. They concern on the skin friction and Nusselt number at different water concentrations and Marangoni effects for the magnetohydrodynamic (MHD)flow of heat transfer over a stretching disk with porous suction and injection. However, Naquib et al. [26] conducted the fluid-flow and heat transfer rate of nanofluid inside a trapezoidal enclosure with a circular heated cylinder. the boundary conditions is in one side of the wall was cooled at constant temperature and the cylinder was placed in different locations inside the enclosure. They observed from results that the location of cylinder has a wide effect on the Marangoni and Rayleigh number. While, Abbas et al. [27] conducted the impact of heat generation on thermal Marangoni convective boundary layer flow of dusty trihybrid nanofluid across a flat surface with thermal radiation and non-linear mixed convection. They discover that their increasing values of Groshof and Marangoni number lead to the skin friction increases too. Also, higher surface tension gradients lead to stronger induced flows and more efficient heat transfer inside the liquid. Leila SAOUDI, and Nordine ZERAIBI [28] investigated the flow of nanofluids in a corrugated channel and the effect on the heat transfer performance. The numerical simulation was conducted using ANSYS-Fluent Software Ver. 16.0 investigating the entropy generation as well as the thermo-hydraulic performance for waving channel taking two corrugation profiles (sinusoidal and square). They observed that the thermodynamic behavior of the Al_2O_3/water nanofluid in different geometries, can be used to enhancement heat transfer in various applications. Ferroud et al. [29] numerically investigation the square fluid-filled cavity for investigation the entropy generation in laminar mixed convection. The side-walls are maintained at a constant temperature Tc, and moving upper ward at a constant velocity. The previous conditions presented to study the effects of irreversibility distribution on the entropy generation for different engineering applications. However, the remaining parts of lower and upper walls are adiabatic. They illustrated that, the total entropy generation increase by increasing the irreversibility distribution ratio and the increase of Prandtl number regardless the values of Ri = 1 and Re = 100.

There has not been a numerical study that deals with free surface square cavities subjected to bottom wall continuous heat flux, according to what has previously been mentioned in the literature. Moreover, it can be used to enhance the solar energy application, which is considered one of the most important branches in the field of renewable energy, in addition to food storage. Therefore, the current work aims to depict the streamlines, isothermal lines, heat lines, and local entropy production for the mixed natural and Marangoni convection in a free surface cavity exposed bottom wall boundary to a constant heat flux. This will enhance the engineering applications and open new application field for square enclosure. Moreover, gives a good imagination about the relation between the applied uniform heat flux over the cavity and the surface tension gradient and its applications for innovate investigation depending on numerical solution of enclosure in point of view the Marangoni effect.

PHYSICAL MODEL EXPLANATION AND GOVERNING EQUATIONS

The cavity had the dimensions L × L with two vertically facing walls that are kept cold (T_c) and an upper free surface that is continuously exposed to both natural and Marangoni convection while a portion of the bottom wall boundary is subjected to a constant heat flux (q'') and other portions are kept adiabatically. The cavity is used in this investigation to test various fluids. Figure (1) illustrates the

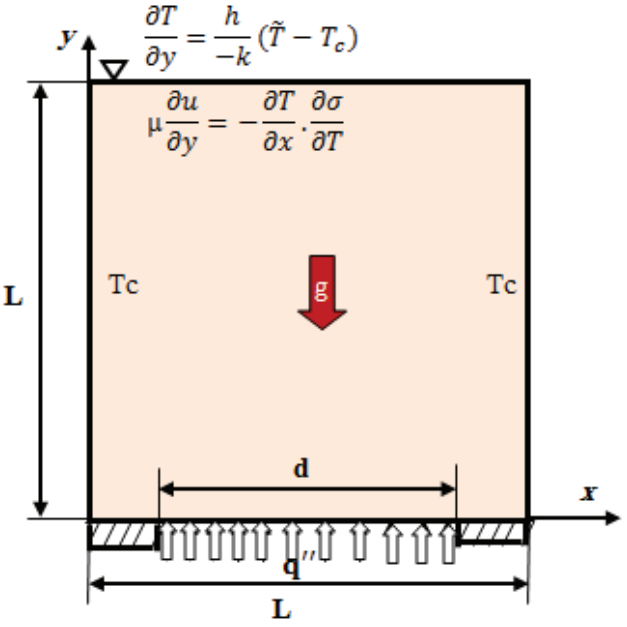

Figure 1. Systematic diagram of physical model.

outline of the schematic drawing of the physical model and its boundaries. Concerning the model, the following broad hypotheses apply:

The fluid flow within the cavity is two-dimensional, steady, and laminar.

1- The fluid in the cavity is Newtonian and incompressible.
2- Gravity works in the opposite direction as the y-axis.
3- The fluid-free surface is flat and perpendicular to the x-axis.
4- Radiative effects are negligible.
5- The velocity along a top-free surface is subject to a slip boundary condition.
6- All fluid parameters remain constant, except for surface tension and density change, which are only temperature-dependent.

Under the aforementioned assumptions, the dimensionless governing equations for the steady natural convection flow in a two-dimensional square cavity can be outlined as:

Conservation of mass [27]:

$$\frac{\partial}{\partial X}\left(\widetilde{U}_i\right)+\frac{\partial}{\partial Y}\left(\widetilde{V}_i\right)=0 \tag{1}$$

Momentium equations:

$$\widetilde{U}_i\frac{\partial}{\partial X}(\widetilde{U}_i)+\widetilde{V}_i\frac{\partial}{\partial Y}(\widetilde{U}_i)=-\frac{\partial}{\partial X}(\tilde{P}_i)+Pr\left(\frac{\partial^2}{\partial X^2}(\widetilde{U}_i)+\frac{\partial^2}{\partial Y^2}(\widetilde{U}_i)\right) \tag{2}$$

$$\widetilde{U}_i\frac{\partial}{\partial X}(\widetilde{V}_i)+\widetilde{V}_i\frac{\partial}{\partial Y}(\widetilde{V}_i)=-\frac{\partial}{\partial Y}(\tilde{P}_i)+Pr\left(\frac{\partial^2}{\partial X^2}(\widetilde{V}_i)+\frac{\partial^2}{\partial Y^2}(\widetilde{V}_i)\right)+Gr\,Pr^2\,\tilde{\theta}_i \tag{3}$$

Energy equations:

$$\widetilde{U}_i\frac{\partial}{\partial X}(\tilde{\theta}_i)+\widetilde{V}_i\frac{\partial}{\partial Y}(\tilde{\theta}_i)=\left(\frac{\partial^2}{\partial X^2}(\tilde{\theta}_i)+\frac{\partial^2}{\partial Y^2}(\tilde{\theta}_i)\right) \tag{4}$$

The following definitions are provided for the non-dimension parameters:

$$X=\frac{x}{L},\quad Y=\frac{y}{L},\widetilde{U}_i=\frac{\tilde{u}_i.L}{\alpha},\widetilde{V}_i=\frac{\tilde{v}_i.L}{\alpha},\tilde{P}_i=\frac{\tilde{p}_iL^2}{\rho\alpha^2},$$
$$\tilde{\theta}_i=\frac{\tilde{T}-T_c}{\Delta T},\Delta T=\frac{q''L}{K},Bi=\frac{(L/k)}{(1/h)},Pr=\frac{\vartheta}{\alpha},$$
$$Gr=\frac{g\beta\,L^3\Delta T}{\vartheta\alpha},\quad \widetilde{Ma}=\frac{\partial\sigma}{\partial T}\frac{q''L^2}{\mu\alpha}$$

$$\widetilde{U}_i=\frac{\partial\tilde{\psi}}{\partial Y},\ \widetilde{V}_i=-\frac{\partial\tilde{\psi}}{\partial X} \tag{5}$$

$$\nabla^2\tilde{\psi}=\frac{\partial^2\tilde{\psi}}{\partial X^2}+\frac{\partial^2\tilde{\psi}}{\partial Y^2} \tag{6}$$

The heat function ($\widetilde{\Pi}_i$), which is derived from convective heat fluxes ($\widetilde{U}_i\tilde{\theta}_i$, $\widetilde{V}_i\,\tilde{\theta}_i$). To represent the heat flow inside the cavity, heat fluxes ($-\frac{\partial\tilde{\theta}_i}{\partial X}$,$-\frac{\partial\tilde{\theta}_i}{\partial Y}$) are utilized.

$$\begin{aligned}\frac{\partial\widetilde{\Pi}_i}{\partial Y}&=\widetilde{U}_i.\tilde{\theta}_i-\frac{\partial\tilde{\theta}_i}{\partial X}\\ -\frac{\partial\widetilde{\Pi}_i}{\partial X}&=\widetilde{V}_i.\tilde{\theta}_i-\frac{\partial\tilde{\theta}_i}{\partial Y}\end{aligned} \tag{7}$$

The differential energy equation for the heat function is given by equation (8) as follows:[15]

$$\frac{\partial^2\widetilde{\Pi}_i}{\partial X^2}+\frac{\partial^2\widetilde{\Pi}_i}{\partial Y^2}=\frac{\partial}{\partial Y}\left(\widetilde{U}_i.\tilde{\theta}_i\right)-\frac{\partial}{\partial X}\left(\widetilde{V}_i.\tilde{\theta}_i\right) \tag{8}$$

In their non-dimensional terms, thermal gradients-induced entropy generation ($\tilde{S}_\theta$) and fluid friction -induced entropy generation ($\tilde{S}_\Psi$) , is defined as[27]:

$$\tilde{S}_{\theta,i}=\left[\left(\frac{\partial\tilde{\theta}_i}{\partial X}\right)^2+\left(\frac{\partial\tilde{\theta}_i}{\partial Y}\right)^2\right] \tag{9}$$

$$\tilde{S}_{\Psi,i}=\Gamma\left[2\left[\left(\frac{\partial\widetilde{U}_i}{\partial X}\right)^2+\left(\frac{\partial\widetilde{V}_i}{\partial Y}\right)^2\right]+\left(\frac{\partial\widetilde{U}_i}{\partial Y}+\frac{\partial\widetilde{V}_i}{\partial X}\right)^2\right] \tag{10}$$

Where Γ is the irreversibility ratio as follows:

$$\Gamma=\frac{\mu.To}{k}\left(\frac{\alpha}{L.\Delta T}\right)^2 \tag{11}$$

To get the total entropy generation, the dimensionless local entropy generation is integrated over the system volume:

$$\widetilde{S_{T,i}}=\int_V\tilde{S}_{\theta,i}.dV+\int_V\tilde{S}_{\Psi,i}\,.dV=\tilde{S}_{\theta,f}+\tilde{S}_{\Psi,f} \tag{12}$$

The following definition applies to the local Nusselt number of the heat sources[17]:

$$Nu=\frac{q''L}{k_f.(T_s-T_c)} \tag{13}$$

The local Nusselt number is rearranged as follows using the temperature dimensionless at heat source wall [26] and [27]:

$$\widetilde{Nu}_i=-\left(\frac{\partial\tilde{\theta}_i}{\partial n}\right)_{wall} \tag{14}$$

Integration of the local Nusselt number along the heat source yields the average Nusselt number ($\overline{\mathrm{Nu}}$) [27]

$$\overline{\mathrm{Nu}}=\frac{1}{D}\int_{(1-\frac{D}{L})/2}^{(1+\frac{D}{L})/2}\widetilde{Nu}_i\,.dX \tag{15}$$

In the current study, the boundary conditions in combination with the governing equations can be written in dimensionless terms as follows[27]:

At vertical walls: $X = 0$ and 1 and $0 \le Y \le 1$

$$\widetilde{U}_i=\widetilde{V}_i=0,\qquad \tilde{\theta}_i=0,\qquad \tilde{\psi}_i=0\,,\qquad n.\nabla\widetilde{\Pi}_i=0$$

At bottom horizontal wall:

$$Y = 0 \; and \;\; (1 - \frac{D}{L})/2 \le X \le (1 + \frac{D}{L})/2$$

$$\widetilde{U}_i = \widetilde{V}_i = 0, \quad \frac{\partial \widetilde{\theta}_i}{\partial Y} = -1, \quad \widetilde{\psi}_i = 0, \quad \frac{\partial \widetilde{\Pi}_i}{\partial X} = -1$$

$$Y = 0 \text{ and } \; 0 \le X \le (1 - \frac{D}{L})/2 \text{ and } \; (1 + \frac{D}{L})/2 \le X \le L$$

$$\widetilde{U}_i = \widetilde{V}_i = \frac{\partial \widetilde{\theta}_i}{\partial Y} = 0, \quad \widetilde{\psi}_i = 0, \quad \widetilde{\Pi}_i = 0$$

At upper free surface of the cavity: $Y = 1$ & $0 \le X \le 1$

$$\widetilde{V}_i = 0, \; \frac{\partial \widetilde{U}_i}{\partial Y} = -\widetilde{Ma} \times \frac{\partial \widetilde{\theta}_i}{\partial X}, \quad \frac{\partial \widetilde{\theta}}{\partial Y} = -Bi \times \widetilde{\theta}_i,$$

$$n.\nabla \widetilde{\Pi}_i = -Bi \times \widetilde{\theta}_i - \widetilde{U}_i \times \widetilde{\theta}_i + \frac{\partial \widetilde{\theta}_i}{\partial X}$$

NUMERICAL METHOD AND VALIDATION

The essential governing equations subject to boundary conditions are numerically integrated by using the finite volume approach, The Tri-Diagonal Matrix Algorithm iteration was utilized to solve the resulting algebraic equations line-by-line. Under the following condition, the iteration process ends [17] and [27]:

$$\chi = \frac{\sum_{i,j} \left| \beta_{i,j}^{t+1} - \beta_{i,j}^{t} \right|}{\left| \beta_{i,j}^{t+1} \right|} \le 10^{-6}$$

where χ is the tolerance; t and β are the iteration number and any of the computed field variables, respectively. The grid pattern used in the current study is uniformly staggered. Grid points of 51 × 51 is used to present the numerical solutions. There are no noteworthy changes in the average heat transfer as the grid size is increased from 51 × 51 to 81 × 81. The fields of the temperature and velocity for the relevant case can therefore be resolved using a grid size of 51 × 51, which has been accepted. In Figure 2, the computational mesh is depicted.

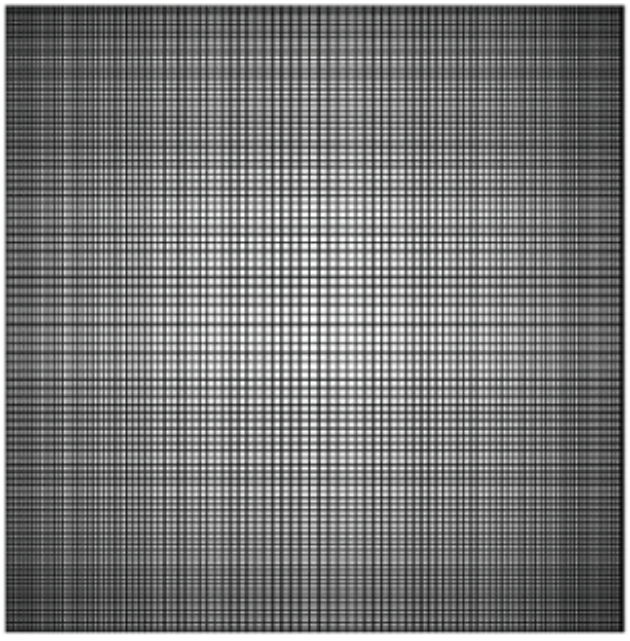

Figure 2. Mesh generation of present study.

There are three validations in this work to show the accuracy of the current results Saleh et al. [3], Ilis et al. [16], and Basak et al. [19]. As shown in Figure 3, Ilis et al. [16], and Basak et al. [19] results were used for the first and second validations of both entropy generation ($\widetilde{S_\psi}$ and $\widetilde{S_\theta}$) in a square cavity with hot left sidewall and cold right sidewall and adiabatic upper and bottom walls. A third validation was performed in accordance with the findings of Saleh et al. [3] in square cavities with an upper free surface. Their results as shown in Figure 4 were simulated for contours of streamlines, isothermal lines, and heatlines, respectively. These findings give reason to believe that the current numerical technique is accurate.

NUMERICAL RESULTS AND DISCUSSION

The results for the contours of isothermal lines, streamlines, heatlines, and entropy generations are indicated for different values of correlated parameters: Grashof number (10^4 to 10^5), Biot number (0 to 80), Prandtl number (0.054, 0.16, 0.71 to 6.22 and 100), and Marangoni number (-10^3 to $+10^4$).

Marangoni Number Effect

For several values of the Marangoni number ($\widetilde{Ma}$ = 0, 5 × 10^2, 1 × 10^3, 3 × 10^3, 5 × 10^3, 10^4), Figure 5 displays streamlines, isothermal lines and heatlines at Bi = 0, ϵ = 1, Gr = 10^4, and Pr = 0.054. The vertical center line of the cavity's cavity is seen to have symmetrical curves. The boundary conditions on the vertical walls are identical and the disregard for convective cooling at the top free surface boundary is the cause of this.

When there is no shear at the free surface ($\widetilde{Ma}$ = 0), surface tension does not affect the flow. As a result, the buoyancy effect mostly governs convection. Because of the different densities of the fluid particles abutting the bottom wall inside the cavity, when the temperature rises, the fluid flow rises from the bottom heated wall along the vertical symmetry axis until it is impeded at the upper free surface, directing the flow horizontally and in opposing directions towards the isothermal cold walls. Then, the flow reverses back straight to the middle region after reaching the bottom wall, falling along the left and right sides of the cold walls. In the left and right halves of the cavity, the flowing fluid, therefore, generates two spinning cells with counterclockwise and clockwise rotations. Because of the decrease in the value of the Grashof number (10^4) and the size of the maximum stream function ($\widetilde{\Psi}_{max}$ = +0.0711), the fluid flow is feeble inside the cavity. When Ma is equal to 500, the effects of surface tension result in the production of secondary flow, which is

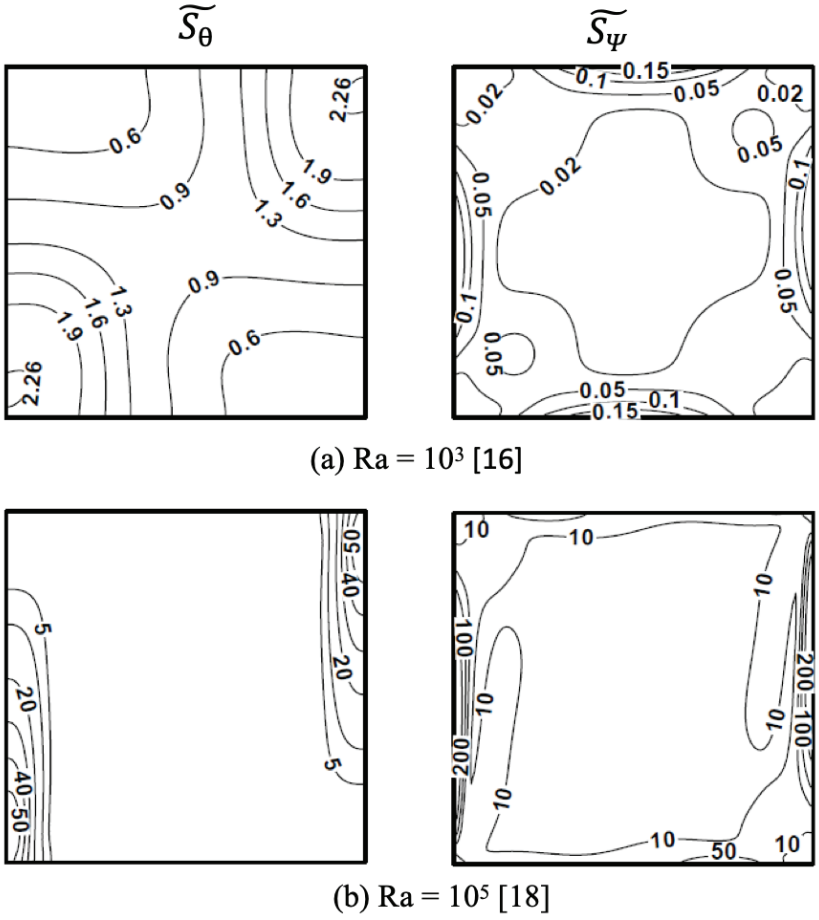

Figure 3. Local entropy generation ($\widetilde{S_\Psi}$ and $\widetilde{S_\theta}$) compared with the results of two sources [16] and [19] at Pr = 0.7.

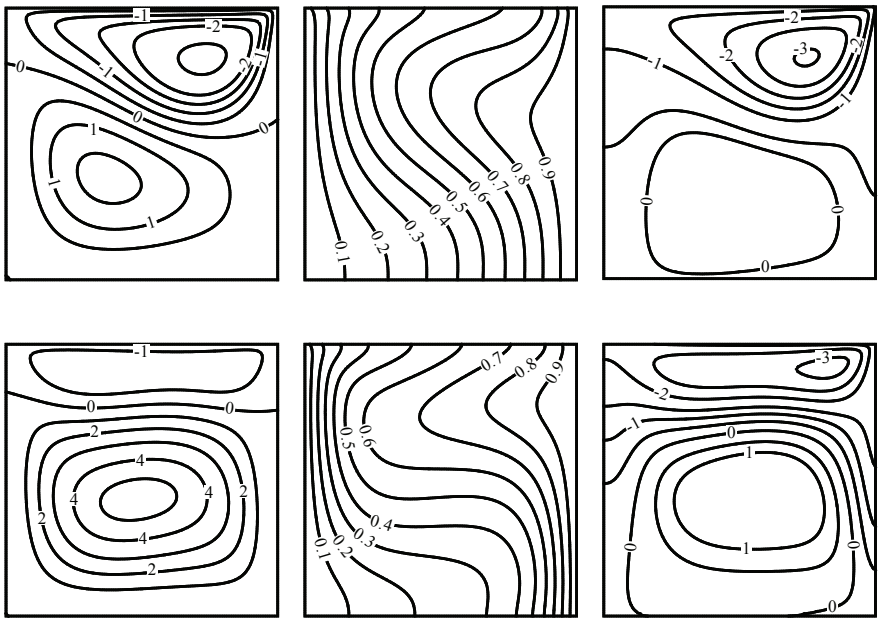

Figure 4. Streamlines, isotherml lines and heatlines, respectively compared with results of Saleh et al. [3] at Gr = 104, Bi = 1 and $\widetilde{\mathrm{Ma}}$ = 103.

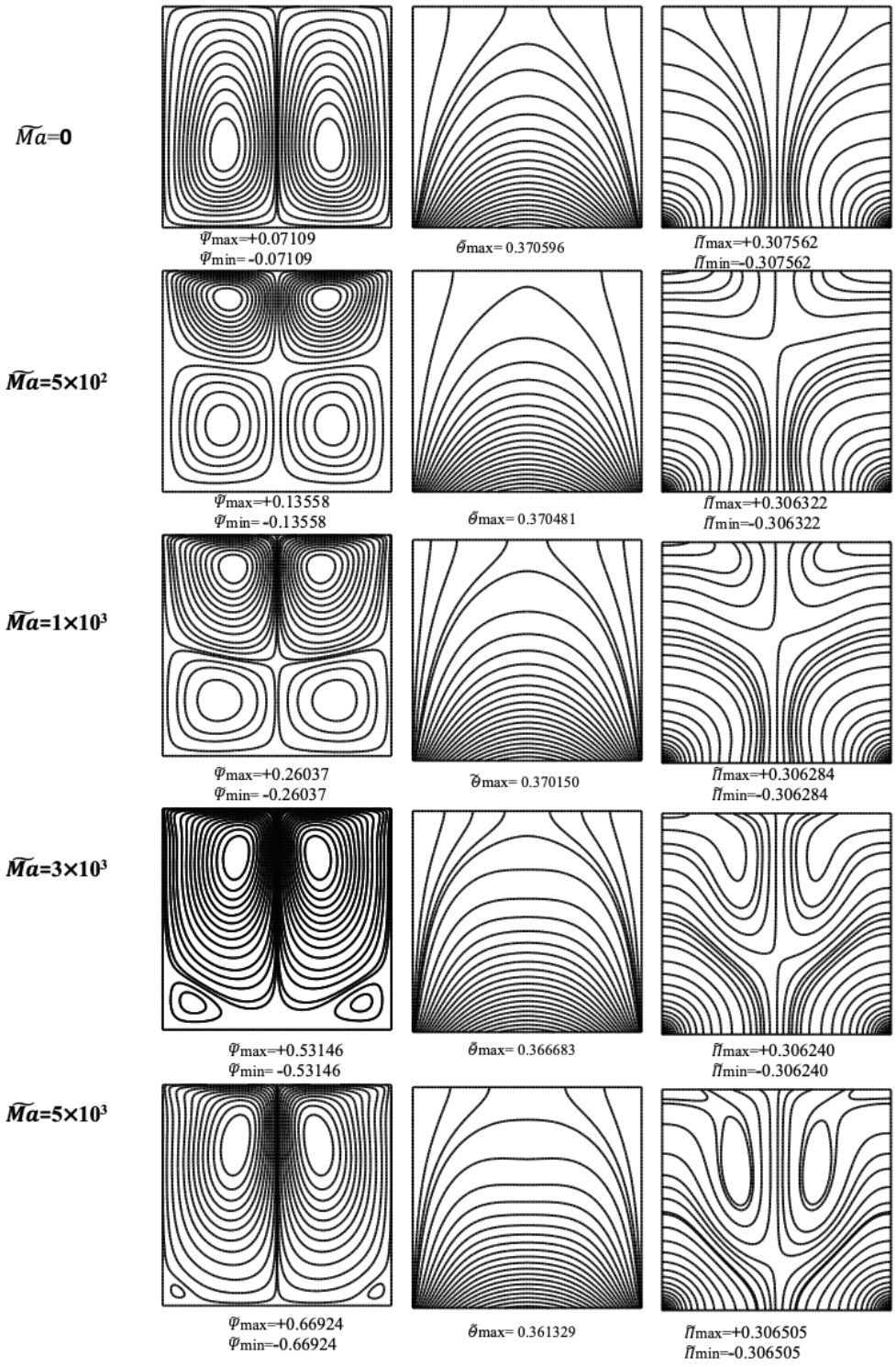

Figure 5. Contours of streamlines, isotherm lines, and heatlines for various Marangoni numbers at Bi = 0, ε = 1, Pr = 0.054 and Gr = 104.

represented at the top free surface by a couple of circulating cells with approximately equal strengths moving in opposite directions. Whereas the major circulating cells at the bottom wall are propelled by buoyancy force. These cells are propelled by thermocapillary forces. As a result, these two forces conflict with one another. Additionally, the streamlines are shown to concentrate on the upper free surface. When the free surface shear stress is reinforced

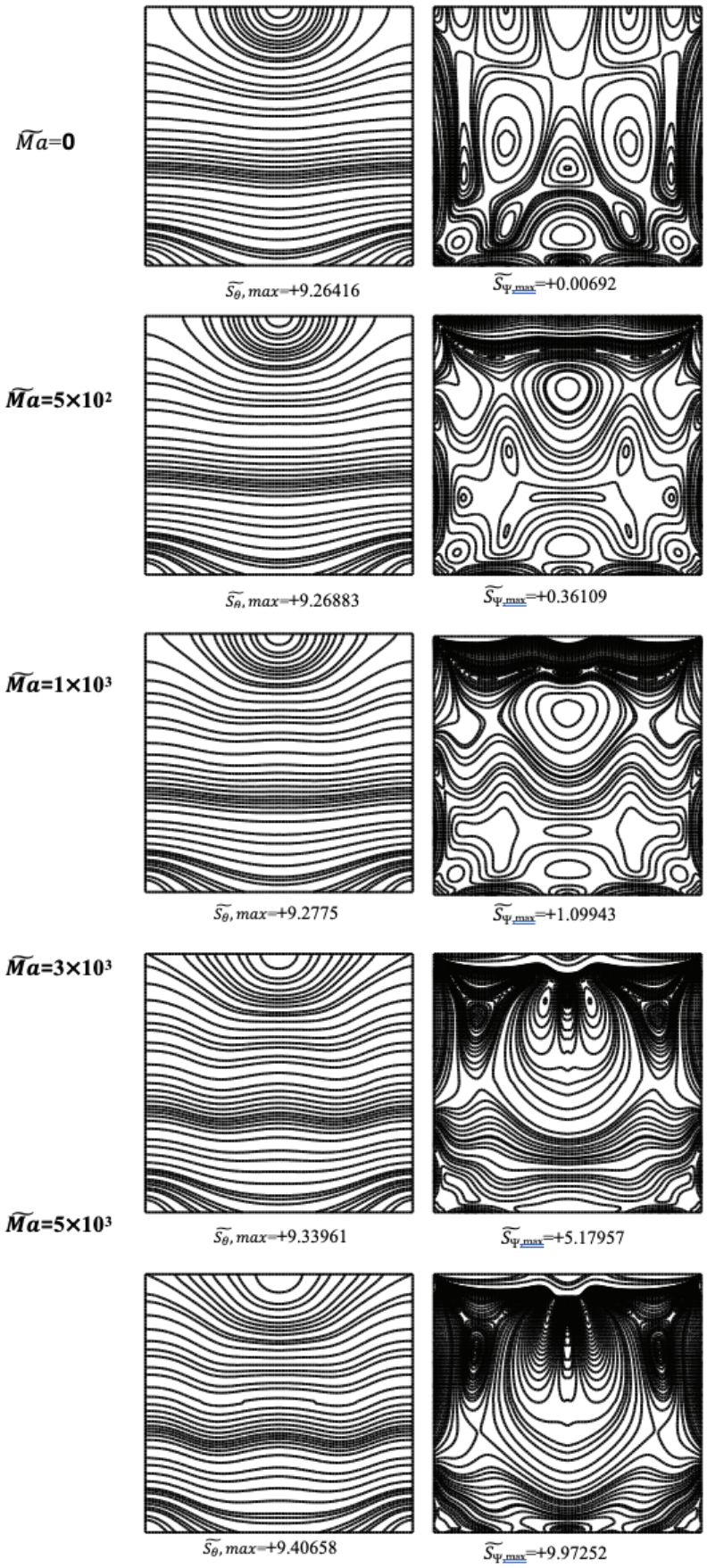

Figure 6. Entropy generation ($\widetilde{S_\theta}$ and $\widetilde{S_\Psi}$) for various Marangoni numbers Bi = 0, ε = 1, Pr = 0.054 and Gr = 104.

($\widetilde{Ma} = 1 \times 10^3$), the free surface velocities increase, and as a result, the buoyant force begins to diminish, and it loses its ability to regulate fluid motion. While the effect of the thermocapillary forces increases, which is represented by a couple of circulating cells at the top free surface. The rotation cells at the top free surface expand inside the enclosing area as Marangoni numbers increase to 3×10^3, which is compressed on a primary cell driven by buoyancy action. When the Marangoni number is raised higher, up to a value of 5×10^3, thermocapillary force takes over the entire domain, making buoyancy force relatively negligible. The two circulation cells as a result take up the whole domain inside the cavity, whereas the two minor corner cells next to the cavity's left and right vertical walls almost shrank and disappeared. The convection that is dominated by the Marangoni effect thus rules in this area. Marangoni convection or thermocapillary flow are two terms used to describe this flow. It can be observed that when Marangoni numbers rise from $\widetilde{Ma} = 0$, $\widetilde{\Psi}_{max} = +0.0711$ to $\widetilde{Ma} = 10^4$, $\widetilde{\Psi}_{max} = +0.88593$), the value of the maximum stream function rises. This tendency is caused by the fact that as the Marangoni number rises, the fluid flow velocity also rises. Because of the significant temperature gradient, as seen in Figure 5, the isothermal lines drop throughout the midplane from bottom to top and concentrate on the hot surface. Additionally, the Marangoni numbers surface (known from the value of $\tilde{\theta}_{max}$) does not effect on the contours of the isothermal lines. The curves of the heatlines show the direction of heat movement inside the cavity. When compared to isothermal line contours, heatlines contours behave differently. Heatlines behave differently for reasons related to intensified thermal mixing. When the surface tension effect is not present, heat flows radiate from the heat flux at the bottom wall and stop at the cold vertical walls. Due to the thermocapillary force, a few heatlines rotate as two swirls at the top corners of the cavity when the surface tension effect is present. These vortices descend in the opposite direction from the direction of heat flow as the Marangoni number increases.

As indicated, the isothermal lines are concentrated near the heat source at the bottom wall, particularly in its corners. Therefore, heat transfer causes the most entropy ($\widetilde{S_{\theta,max}}$) to be formed at the corners of the bottom wall. The findings shown in Figure 6 demonstrated that as Marangoni numbers increase, the generation of entropy due to heat transfer increases. (i.e. $\widetilde{Ma} = 0$ to $\widetilde{Ma} = 5 \times 10^3$; $\widetilde{S_{\theta,max}} = +9.2642$ to $\widetilde{S_{\theta,max}} = +9.4066$). On the other hand, the large, intense flow, except in the scenario where $\widetilde{Ma}$ is equal to zero, causes the entropy generation caused by fluid friction to concentrate on the free surface. The generation of entropy resulting from fluid friction is likewise increased as thermal Marangoni numbers rise. ($\widetilde{S_{\Psi,max}} = +0.0069$ for $\widetilde{Ma} = 0$ to $\widetilde{S_{\Psi,max}} = +9.973$ for $\widetilde{Ma} = 5 \times 10^3$). Which is very crucial for improving many engineering applications that depends on Marangoni numbers.

Prandtl Number Effect

Five values of the Prandtl number are taken into account in order to conduct a thorough investigation: Pr = 0.71 for air, Pr = 6.2 for water at 25 °C, Pr = 100 for motor oil at 20 °C and finally Pr= 0.054, and 0.16 for liquid metals. For different Prandtl values at $\widetilde{Ma} = 10^3$, Bi = 1, ε = 1, and Gr = 10^5, Figure 7 displays streamlines, isothermal lines and heatlines. These contours are asymmetrical about the cavity's vertical center line due to the convective cooling effect at the upper boundary.

Because there is no wall at the top free surface, as illustrated in Figure 7 (Pr = 0.054), the maximum velocity profile appears there. As a result, the streamlines around the cavity's center show the appearance of a counter-rotating cell. Near the top-left corner of the free surface, the fluid flow encounters the rotation cell and then reverses direction. The temperature there is significantly non-uniform due to the high velocity near the free surface, particularly in the top-left corner. The flow is largely motionless on the opposite side towards the bottom-right corner which causes little secondary clockwise circulations. A slight Prandtl number effect is evident at the top free surface due to the impact of surface tension. When Pr = 0.16, the size of the bottom cell increases as a result of the buoyancy effect, whereas the size of the top circulation cells caused by surface tension decreases. The top rotating cells are compressed and equal in size within the cavity as a result of the buoyancy effect as Pr is raised to 0.71, which causes a further drop in the thermocapillary force effect. Since both driving forces have similar magnitudes, combined convection is likely to occur, as demonstrated in the instance of Pr to 0.71. The buoyancy effect grows more rapidly than the thermocapillary effect when Pr approaches 6.2. With $\widetilde{\Psi}_{max} = +11.974$, it can be seen that the fluid velocities are higher and happen just below the free surface. The magnitudes of the stream function are found to be stronger when Pr is increased to 100 ($\widetilde{\Psi}_{max} = +34.683$). Because buoyancy-driven convection rather than thermocapillary convection is more prevalent, the fluid motion tends to the left. As you get closer to the walls, the isothermal lines get denser, indicating increased heat transfer from the heated bottom wall to the top parts of the side walls. It has been noted that the contours of streamlines and heatlines are identical. Additionally, because of the increased thermal mixing within the cavity, the size of the heat function grows with increasing Pr. On the other hand, Figure 8 indicated entropy generation caused by temperature gradients and fluid friction for different Prandtl values at $\widetilde{Ma} = 10^3$, Bi = 1, ε = 1, and Gr = 10^5. Where contours of S_θ are concentrated, there is a high value of S_θ for entropy generation resulting from heat transfer near hot places. Due to fluid friction, the cool side walls also function as potent entropy-generating sites. Along the middle of the side walls, $\widetilde{S_\Psi}$ is at its highest value. Intriguingly, the amount of entropy generated by fluid friction barely increases as the Prandtl number rises (i.e. $\widetilde{S_{\Psi,max}} = +3.4936$ for Pr = 0.054 to $\widetilde{S_{\Psi,max}} = +37.23$ for Pr=0.71). As observed from $\widetilde{S_{\Psi,max}}$

contours along the vertical centerline with $\widetilde{S_{\Psi,max}}$ = 399.217 to $\widetilde{S_{\Psi,max}}$ = +12519.3 for Pr = 6.2 to 100, results of $\widetilde{S_{\Psi,max}}$ in large entropy formation at higher Pr due to the inclination of counter-rotation of circulation cells. As Pr increases from Pr = 0.015 to Pr = 100, the entropy generated by heat transfer reduces from $\widetilde{S_{\Psi,max}}$ = +9.3734 to $\widetilde{S_{\Psi,max}}$ = +3.9269.

Biot Number Effect

Figure 9 depicts the contours of streams for various values of Biot number (Bi = 0, 5, 10, 40, 80) for Pr = 0.054, Gr = 10^5 for the two cases: (a) $\widetilde{Ma}$ = $+10^4$ and (b) $\widetilde{Ma}$ = -10^3. The Bi is crucial to the mechanism of heat transfer. In the situation of $\widetilde{Ma}$ = $+10^4$, it is believed that the surface tension decreases with increasing temperature. A huge anticlockwise rotating cell and a small clockwise rotating cell respectively appear towards the center and top corner of the cavity when there is no convective cooling effect (Bi = 0). This is brought on by a significant influence of surface tension and a large temperature gradient near the free surface. Because of the thermal gradient difference between the cold and hot

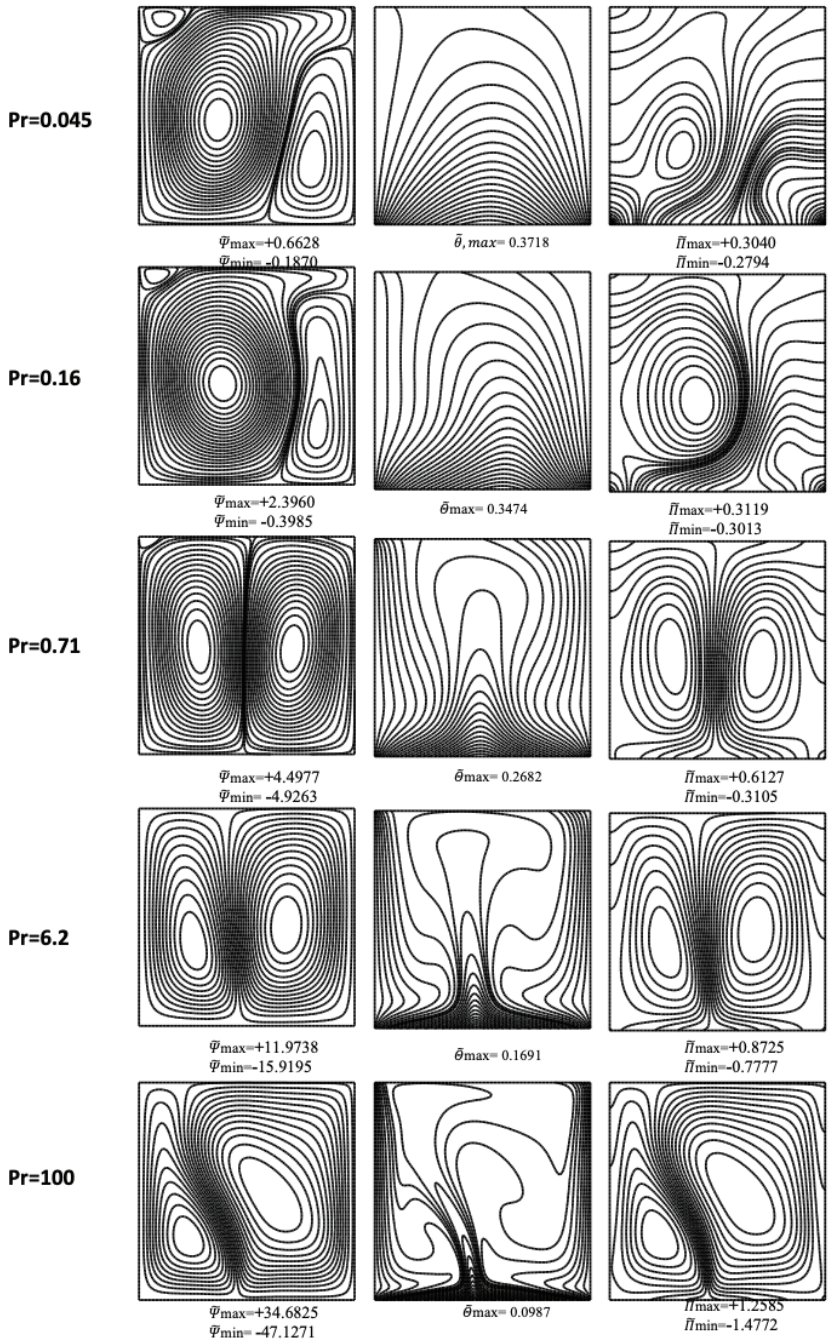

Figure 7. Contours of streamlines, isotherms and heatline for various Prandtl numbers at Bi=1, ε=1, $\widetilde{Ma}$ = 10^3, and Gr=10^5.

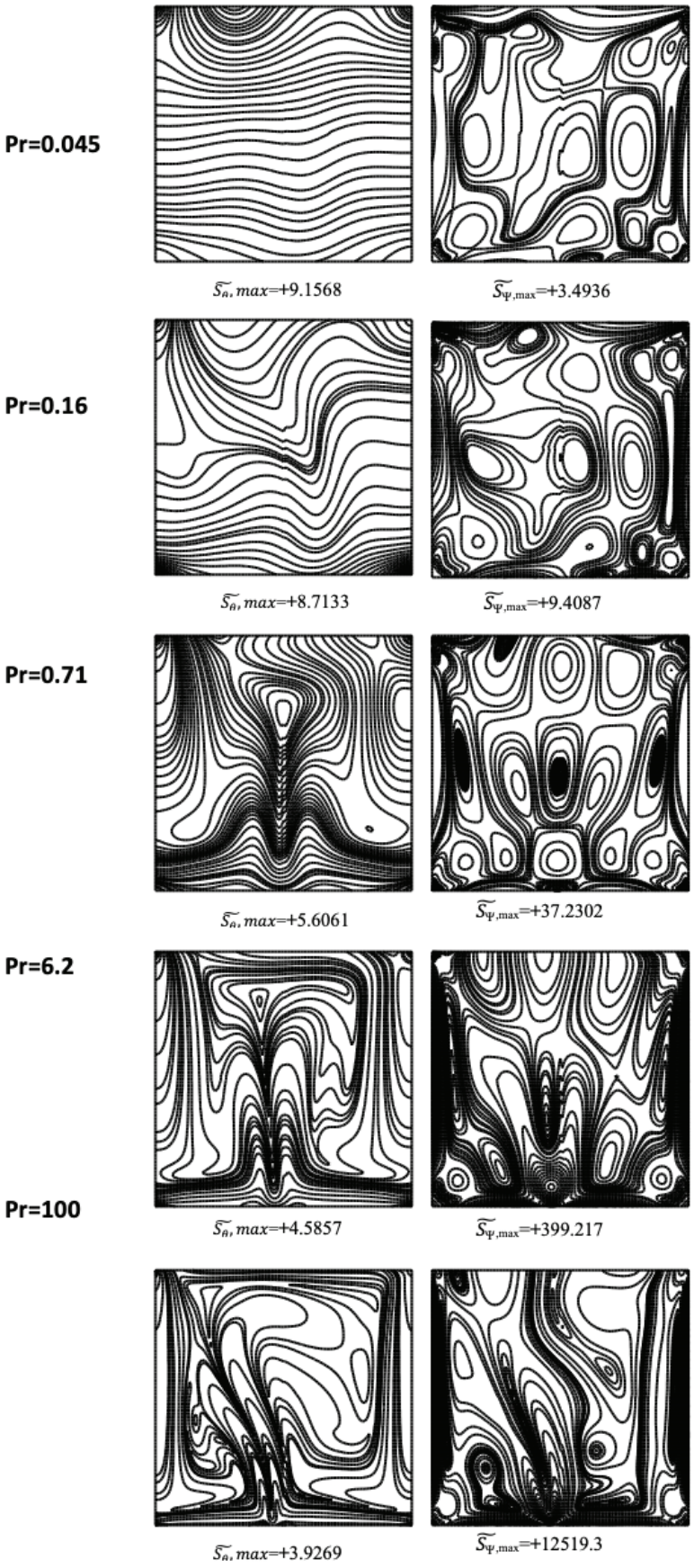

Figure 8. Entropy generation (Sθ and SΨ) for different Prandtl numbers at Bi=1, ε=1, Gr=105 and $\widetilde{\mathrm{Ma}}$ = 103.

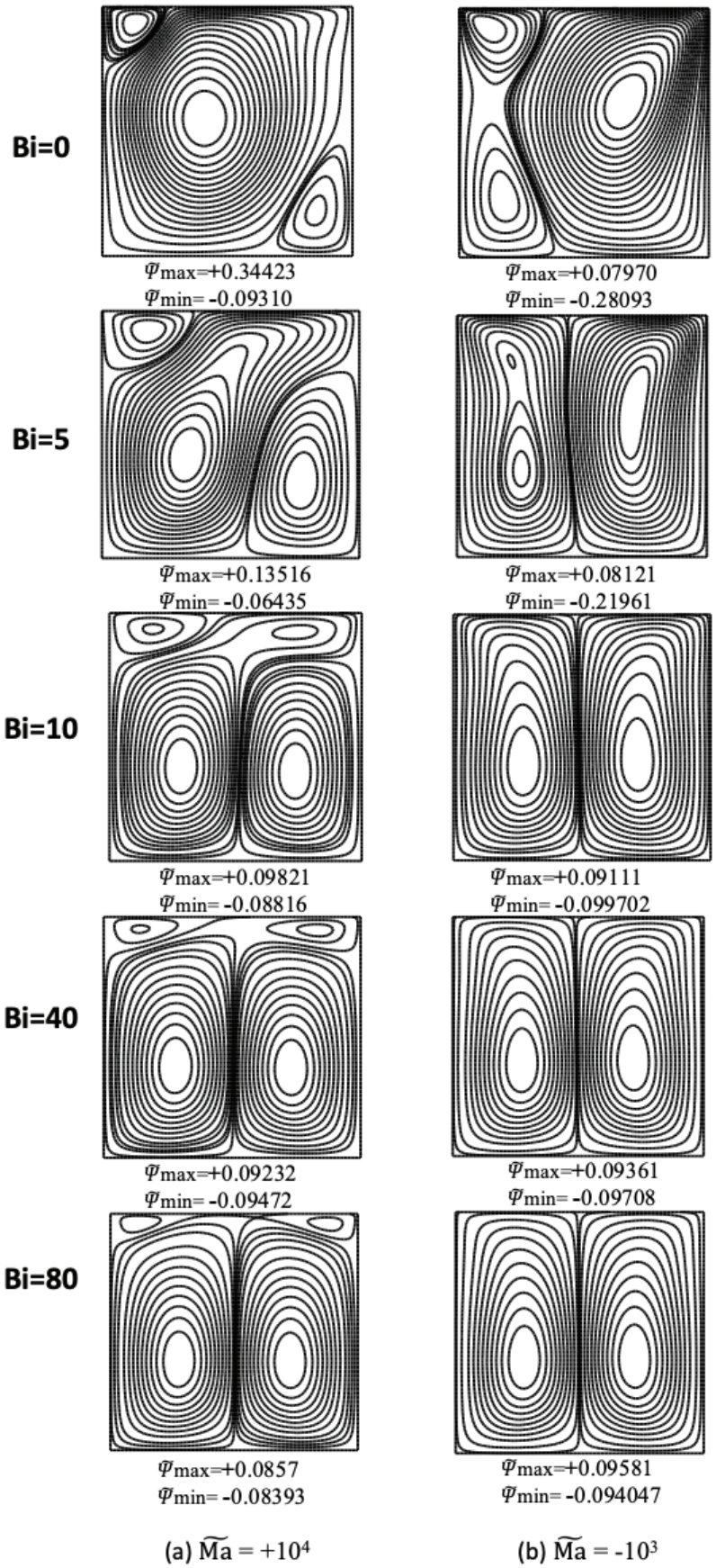

Figure 9. Streamlines contours for various Biot numbers at Gr=105, Pr = 0.054 for two cases: (a) $\widetilde{Ma}$ = +104 and (b) $\widetilde{Ma}$ = -103

walls, a small clockwise spinning cell forms at the right bottom wall corner. As the heat transfer rate improves for (Bi = 5), the circulation cell near the right corner of the bottom wall starts to enlarge. The buoyancy effect dominates fluid motion for (Bi = 10) because the convective cooling at the top free surface rises. Surface tension has a weaker impact as the Biot number increases (40–80), definitely as a result of increased convection cooling at the upper free surface. When the Marangoni number is negative ($\widetilde{Ma} = -10^3$), the fluid motion slows down and a clockwise streamline cell concentration occurs at the left cold wall (Bi = 0). The exterior convection resistance lowers for high Biot numbers (Bi = 5), which improves both transfer rates. When the surface tension is negligible, changing the Biot number which ranges from 10, 40, and 80 does not significantly affect the flow pattern. When $Gr = 10^5$, buoyancy forces for the same Marangoni number values become stronger.

CONCLUSION

The following are the primary conclusions:

1- When there is no convection cooling impact on the top free surface, the maximum stream function values increase as the Marangoni number grows, but the isotherm contours are unresponsive to this change. However, as the Marangoni number rises, the quantity of entropy that produced by heat convection and fluid friction also increases.
2- The heatlines, stream functions and entropy generation due to fluid friction all increase as the Prandtl number do, however, isothermal lines and entropy generation owing to heat transfer reduce as the Pr number rises under similar conditions.
3- For small values of Biot number, the effect of surface tension on fluid motion is considerable; but it is weak for large Biot numbers.
4- In this research raises in marangoni will help to undiminished of heat translated and induced several types of vortices that may enhance free convection, which maximize the heat transfer and improves its utilization.
5- There are clear impact of the value of Prandtl on the entropy distribution from the value 0.16 to 0.7.
6- Recommendations

This work can be modified by presented many types of noise that may produce other effects on flow parameters in duct, the research in following areas cab be recommended.

1. Using directly the square enclousure with marangoni applications in solar collector in such away for decrease the power required for industrial applications.
2. Using more that one working fluid like gas with water for investigations the effect of marangoni number.
3. There many enclosure shapes can numerically anlyzied and may give more efficient for natural convection with marangoni.

NOMENCLATURE

C_p	Specific heat at constant pressure (kJ/kg.K)
D	Cavity characteristic length m
g	Gravitational acceleration (m/s^2)
k	Thermal conductivity (W/m.K)
L	Height or Width of the cavity (m)
P	Dimensionless pressure
p	Pressure (Pa)
Pr	Prandtl number (ϑ/α)
q''	Heat flux (W/m^2)
Ra	Rayleigh number ($g\beta L^3 \Delta T/\vartheta\alpha$)
T	Temperature (K)
T_c	Temperature of the cold surface (K)

Greek symbols

α	Thermal diffusivity (m^2/s)
θ	Dimensionless temperature (T-Tc/ΔT)
$\widetilde{\Psi}$	Dimensional stream function (m^2/s)
$\tilde{\psi}$	Dimensionless stream function
μ	Dynamic viscosity (kg.s/m)
ϑ	Kinematic viscosity (μ/ρ) (m^2/ s)

Subscripts

c	Cold
h	Hot

Abbreviations

$\widetilde{Ma}$	Marangoni number
Min	Minimum
b	Base heat source
$\overline{Nu}$	Local Nusselt number on the heat source surface
$\overline{Nu}_s$	Average Nusselt number along the heat source
$\widetilde{U}$	Dimensionless velocity component in x-direction
$\tilde{u}$	Velocity component in x-direction (m/s)
$\widetilde{V}$	Dimensionless velocity component in y-direction
$\tilde{v}$	Velocity component in y-direction (m/s)
X	Dimensionless coordinate in horizontal direction
x	Cartesian coordinate in horizontal direction (m)
Y	Dimensionless coordinate in vertical direction
y	Cartesian coordinate in vertical direction (m)”
ε	Ratio of heating element length to the cavity height (%)
$\widetilde{\Pi}$	Heatfunction
ΔT	Ref. temperature difference (q” L/k)
β	Volumetric coefficient of thermal expansion (K^{-1})
ρ	Density (kg/m^3)

AUTHORSHIP CONTRIBUTIONS

Authors equally contributed to this work.

DATA AVAILABILITY STATEMENT

The authors confirm that the data that supports the findings of this study are available within the article. Raw data that support the finding of this study are available from the corresponding author, upon reasonable request.

CONFLICT OF INTEREST

The author declared no potential conflicts of interest with respect to the research, authorship, and/or publication of this article.

ETHICS

There are no ethical issues with the publication of this manuscript.

STATEMENT ON THE USE OF ARTIFICIAL INTELLIGENCE

Artificial intelligence was not used in the preparation of the article.

REFERENCES

[1] Song T, Comparison of Buoyancy and Surface Tension in a Square Cavity. Springer 1991;5:10−15. [CrossRef]

[2] Priede J, Cramer A, Bojarevics A, Gelfgat AY, Bar-Yoseph PZ, Yarin AL. Gunter Gerbeth, Experimental and numerical study of anomalous thermocapillary convection in liquid gallium. Phys Fluids 1999;11:3331−3339. [CrossRef]

[3] Saleh H, Arbin N, Roslan R, Hashim I. Visualization and analysis of surface tension and cooling effects on differentially heated cavity using heatline concept. Int J Heat Mass Transf 2012;55:6000−6009. [CrossRef]

[4] Bergman TL, Ramadhyani S. Combined buoyancy and thermocapillary driven convection in open square cavities. Numer Heat Transf 1986;9:441−451. [CrossRef]

[5] Cicek K, Baytas AC. A Numerical Study of Combined Natural and Marangoni Convection in a Square Cavity. TransNav 2009;3. [CrossRef]

[6] Strani M, Piva R, Graziani G. Thermocapillary convection in a rectangular cavity: asymptotic theory and numerical simulation. J Fluid Mech 1983;130:347−376. [CrossRef]

[7] Arbin N, Saleh H, Hashim I, Chamkha AJ. Numerical investigation of double-diffusive convection in an open cavity with partially heated wall via heatline approach. Int J Therm Sci 2016;100:169−184. [CrossRef]

[8] Jue TC. Combined thermosolutal buoyancy and surface-tension flows in a cavity. Heat Mass Transf 1999;35:149−161. [CrossRef]

[9] Rudraiah N, Venkatachalapp M, Subbaraya CK. Combined Surface Tension and Buoyancydriven Convection in a Rectangular Open Cavity in the Presence of a Magnetic Field. Int J Non-linear Mech 1995;30:759−770. [CrossRef]

[10] Saleem M, Hossain MA, Hafiz MZ. Effect of Magnetic Field on Double Diffusive Marangoni Convection with Chemical Reaction in a Square Cavity. Available at: https://me.buet.ac.bd/public/old/icme/icme2011/Proceedings/PDF/ICME%2011-FL-002.pdf. Accessed on 5 Mar 2026.

[11] Hossain MA, Hafiz MZ, Rees DAS. Buoyancy and thermocapillary driven convection flow of an electrically conducting fluid in an enclosure with heat generation. Int J Therm Sci 2005;44:676−684. [CrossRef]

[12] Oztop HF, Lioua K, Mohamad NB, Al-Salem K. Numerical study of three-dimensional combined buoyancy and thermocapillary convection and evaluation of entropy generation. Available at: www.emeraldinsight.com/0961-5539.htm. Accessed on 5 Mar 2026.

[13] Saleh H, Hasmim I. Buoyant Marangoni convection of nanofluids in square cavity. Appl Math Mech Engl Ed 2015;36:1169−1184. [CrossRef]

[14] Saleem M, Hossain MA, Mahmud S, Pop I. Entropy generation in Marangoni convection flow of heated fluid in an open ended cavity. Int J Heat Mass Transf 2011;54:4473−4484. [CrossRef]

[15] Basak T, Singh AK, Sruthi TPA, Roy S. Finite element simulations on heat flow visualization and entropy generation during natural convection in inclined square cavities. Int Commun Heat Mass Transf 2014;51:1−8. [CrossRef]

[16] Ilis G, Mobedi M, Sunden B. Effect of aspect ratio on entropy generation in a rectangular cavity with differentially heated vertical walls. Int Commun Heat Mass Transf 2008;35:696−703. [CrossRef]

[17] Bouabid M, Magherbi M, Hidouri N, Brahim AB. Entropy generation at natural convection in an inclined rectangular cavity. Entropy 2011;13:1020−1033. [CrossRef]

[18] Ahmed SE, Oztop HF, Elshehabey HM. Thermosolutal Marangoni convection of Bingham non-Newtonian fluids within inclined lid-driven enclosures full of porous media. Heat Transf 2021;50:7898−7917. [CrossRef]

[19] Kolsi L, Algarni S, Mohammed HA, Hassen W, Lajnef E, Aich W, et al. 3D Magneto-Buoyancy-Thermocapillary Convection of CNT-Water Nanofluid in the Presence of a Magnetic Field. Processes 2020;8. [CrossRef]

[20] Basak T, Gunda P, Anandalakshmi R. Analysis of entropy generation during natural convection in porous right-angled triangular cavities with various thermal boundary conditions. Int J Heat Mass Transf 2012;55:4521−4535. [CrossRef]

[21] Bobach BJ, Boman R, Celentano D, Terrapon VE, Ponthot JP. Simulation of the Marangoni Effect and Phase Change Using the Particle Finite Element Method. Appl Sci 2021;11:11893. [CrossRef]

[22] Siri Z, Al 'Idrus SNSMN. Marangoni convection in a C-shape enclosure with partially heated walls. J Phys 2023;2633:012016. [CrossRef]

[23] Zisan HMTA, Ruvo TH, Saha S. Marangoni Natural Convection in a Discretely Heated Cubic Cavity under Isoflux Heating Condition. Available at: http://ieomsociety.org/proceedings/2021dhaka/413.pdf. Accessed on 5 Mar 2026.

[24] Muhammad ASNBNS, Bin SZ, Habibis S. Marangoni convection in a trapezoidal enclosure with a heated circular cylinder. Therm Sci 2025;29:567−577. [CrossRef]

[25] Omer ASA. Marangoni Convection in Hybrid Nanofluid Flow over a Disk. Eur J Pure Appl Math 2025;18:1307−5543. [CrossRef]

[26] Muhammad ASNBNS, Bin SZ, Habibis S. Marangoni convection in a trapezoidal enclosure with a heated circular cylinder. Therm Sci 2025;29:567−577. [CrossRef]

[27] Abbas M, Khan N, Hashmi MS, Alhefthi RK, Rezapour S, Ince M. Thermal Marangoni convection in two-phase quadratic convective flow of dusty MHD trihybrid nanofluid with non-linear heat source. Case Stud Therm Eng 2024;57:104190. [CrossRef]

[28] Saoudi L, Zeraibi N. Entropy generation of Al2O3/water nanofluid in corrugated channels. J Therm Eng 2023;9:885−900. [CrossRef]

[29] Ferroudj N, Köten H. Numerical Simulation Of Prandtl Number Effect on Entropy Generation in a Square Cavity. J Therm Eng 2021;7:1016−1029. [CrossRef]